Article

Brownian Force Profile Reconstruction of Interfacial 1-Nonanol Solvent Structure

Paul D. Ashby, and Charles M. Lieber

J. Am. Chem. Soc., **2004**, 126 (51), 16973-16980• DOI: 10.1021/ja045970r • Publication Date (Web): 04 December 2004

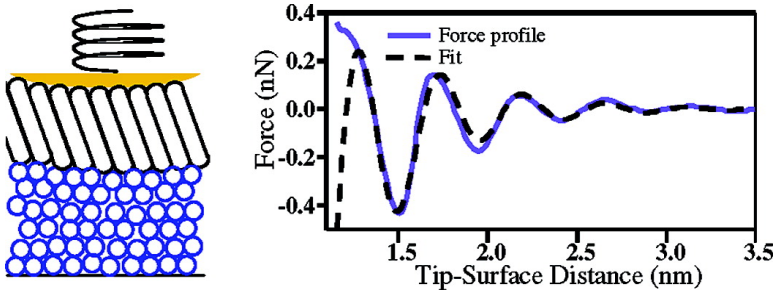

More About This Article

Additional resources and features associated with this article are available within the HTML version:

- Supporting Information
- Links to the 1 articles that cite this article, as of the time of this article download
- Access to high resolution figures
- Links to articles and content related to this article
- Copyright permission to reproduce figures and/or text from this article

View the Full Text HTML

J|A|C|S
ARTICLES
Published on Web 12/04/2004

Brownian Force Profile Reconstruction of Interfacial 1-Nonanol Solvent Structure

Paul D. Ashby*,† and Charles M. Lieber

Contribution from the Department of Chemistry and Chemical Biology, Harvard University, Cambridge, Massachusetts 02138

Received July 6, 2004; E-mail: pashby@cmliris.harvard.edu

Abstract: Using Brownian force profile reconstruction (BFPR), we measured the solvent structure force profile of interfacial 1-nonanol between graphite and methyl terminated alkane thiol SAM surfaces. BFPR harnesses the thermal motion of the cantilever to accurately and precisely reconstruct force profiles that may be stiffer than the intrinsic cantilever stiffness. Novel methods to compensate instrument noise and seamlessly stitch together subsections of the force profile significantly improve upon previous reconstruction techniques using thermal noise. The increased accuracy and precision of BFPR could enable the measurement of stiff or rough energy landscapes such as solvent structure or ligand−protein binding. The force profile for interfacial 1-nonanol solvent structure was well fit by an exponentially decaying sinusoid function with a period of 4.5 Å for distances greater than four molecular layers, revealing liquid behavior. Distances shorter than four molecular layers displayed solid behavior with interlayer transitions being 3.9 Å and possible crystal orientation rearrangements causing submolecular steps upon subsequent confinement.

Introduction

Energy landscapes and force profiles guide all intermolecular and interfacial interactions and thus are the focus of years of interdisciplinary research because of their central importance in physics, chemistry, and biology. Indirect analysis techniques dominate most of the investigation into the characteristics of interfacial interactions,[1] but direct measurement of complete force profiles promises to be the most informative and allow the derivation of other physical properties.

The methods for directly measuring force profiles and energy landscapes can initially be split into two technique categories: oscillatory and static deflection. Oscillatory techniques, such as force modulation atomic force microscopy (FMAFM), drive the probe near the sample in the spring's harmonic potential and use the phase, amplitude, and oscillation frequency to determine the potential.[2−7] Frequency detection is more accurate in a low damping environment, causing the implementation of FMAFM to be very difficult in solution, where the majority of interesting samples are investigated. Static deflection techniques measure spring deflection at low frequencies and use Hooke's law to calculate force. Static deflection techniques have been the foundation of force measurements for decades.

The surface forces apparatus (SFA) was the first interfacial force measurement instrument to gain wide popularity due to its excellent absolute position resolution and force sensitivity. Pioneering experiments performed with the SFA led to the characterization of van der Waals, electrostatic, adhesive, and hydration forces.[8] Invention of the atomic force microscope (AFM),[9] with its ultrasharp probe and superior, yet relative, position resolution, promised to significantly advance force profile measurement and enable single molecule experiments.[10−13] Historically, these methods have used relatively weak springs, compared to the stiffness of the interaction, to increase the force sensitivity. Unfortunately, the measurements traded force profile information for increased force sensitivity as the spring experienced instabilities for most interactions and followed trajectories off the equilibrium energy surface.

Three recent theoretical developments reconstruct information about the energy landscape from nonequilibrium measurements. First, Evans and co-workers reformulated Kramer's reaction rate theory to determine barrier heights and distances by measuring unbinding forces at different loading rates.[14] Application of this theory shed insight into ligand−receptor binding[15,16] and protein folding.[10,17] Second, Jarzynski derived an expression for the

† Current address: Molecular Foundry, Lawrence Berkeley National Laboratory, Berkeley, CA, 94720.

(1) Birdi, K. S., Ed. *Handbook of Surface and Colloid Chemistry*, 2nd ed.; CRC Press: Boca Raton, FL, 2003.
(2) Sader, J. E.; Jarvis, S. P. *Appl. Phys. Lett.* **2004**, *84*, 1801−1803.
(3) Holscher, H.; Gotsmann, B.; Schirmeisen, A. *Phys. Rev. B* **2003**, *68*.
(4) Holscher, H.; Allers, W.; Schwarz, U. D.; Schwarz, A.; Wiesendanger, R. *Phys. Rev. Lett.* **1999**, *83*, 4780−4783.
(5) Gotsmann, B.; Kruger, D.; Fuchs, H. *Europhys. Lett.* **1997**, *39*, 153−158.
(6) Gotsmann, B.; Anczykowski, B.; Seidel, C.; Fuchs, H. *Appl. Surf. Sci.* **1999**, *140*, 314−319.
(7) Gotsmann, B.; Fuchs, H. *Phys. Rev. Lett.* **2001**, *86*, 2597−2600.
(8) Isaelachvili, J. *Intermolecular and Surface Forces*, 2nd ed.; Academic Press: San Diego, CA, 1992.
(9) Binnig, G.; Quate, C. F.; Gerber, C. *Phys. Rev. Lett.* **1986**, *56*, 930−933.
(10) Williams, P. M.; Fowler, S. B.; Best, R. B.; Toca-Herrera, J. L.; Scott, K. A.; Steward, A.; Clarke, J. *Nature* **2003**, *422*, 446−449.
(11) Wong, S. S.; Joselevich, E.; Woolley, A. T.; Cheung, C. L.; Lieber, C. M. *Nature* **1998**, *394*, 52−55.
(12) Wong, S. S.; Woolley, A. T.; Joselevich, E.; Cheung, C. L.; Lieber, C. M. *J. Am. Chem. Soc.* **1998**, *120*, 8557−8558.
(13) Zhuang, X. W.; Rief, M. *Curr. Opin. Struct. Biol.* **2003**, *13*, 88−97.
(14) Evans, E.; Ritchie, K. *Biophys. J.* **1997**, *72*, 1541−1555.
(15) Merkel, R.; Nassoy, P.; Leung, A.; Ritchie, K.; Evans, E. *Nature* **1999**, *397*, 50−53.

equilibrium free energy difference from an ensemble of measurements of the nonequilibrium work.[18] Bustamante and co-workers tested the equality by pulling RNA molecules both at quasi-equilibrium and nonequilibrium.[19] Hummer and Szabo applied the same ideas as the Jarzynski equality to calculate much of the equilibrium energy surface from nonequilibrium work measurements.[20] Third, Todd and Eppell developed a method for reconstructing the force profile from inversion of the trajectory during snapping.[21,22] Unfortunately, the method struggles with amplification of the noise in the inversion process.[23] These methods address the needs of the force spectroscopy community to extract useful information from pulling experiments with weak springs, but in all three cases the fast transition over the barrier reduces the amount of time that information about the transition region is collected to only a few microseconds per force curve. This short collection time in this region reduces the precision of the force profile or energy landscape. Thus, a solution to the difficulty of accurately measuring the whole force profile is to increase the spring constant and perform a quasi-equilibrium measurement, where the transition region can be sampled for tens of milliseconds.

Some researchers attempted quasi-equilibrium experiments while keeping the force sensitivity of weak springs by using feedback to electronically stiffen the cantilever. As early as the 1950s, Derjaguin used a feedback system to stabilize the distance for measuring attractive dispersion forces.[24] Houston made advances in sensitivity by developing the interfacial force microscope, which was used to measure alkane thiol SAM compressibility.[25−27] Similarly, Stewart and Parker developed feedback for the SFA, which increased the stiffness many orders of magnitude until they were only limited by complexities in the motion of their force sensor and apparatus.[28] Using magnetic force feedback for AFM measurements further resolved strong physical interactions in air or vacuum[29−32] and chemical interactions in solution.[33] Contrary to its original intention, the feedback loop decreased overall sensitivity because the feedback added detection noise and did not control the cantilever motion near the resonance.[34] Feedback experiments thus suggest that intrinsically stiff springs are required to measure the whole force profile.

Using springs with stiffness near the stiffness of the interaction enables the cantilever to sample the interaction without instability, and as a result, the thermal motion of the cantilever is dictated by the tip−surface energy landscape combined with the cantilever harmonic well. Instead of being a source of signal degradation, the thermal noise contains information about the tip−surface interaction and for cantilever quality factor, Q, greater than one the thermal noise deflections are more easily measured above the instrument noise than the static deflection near DC. Deciphering the cantilever thermal noise requires relating the thermal motion to the tip−surface interaction through the equation for a Boltzmann distribution,

$$U(z) = -k_B T \ln(p(z)) + C \quad (1)$$

where $U(z)$ is the free energy as a function of the tip−surface distance, k_B is Boltzmann's constant, T is temperature, $p(z)$ is the cantilever position probability density distribution, and C is a constant. Cleveland and co-workers first harnessed this information to observe perturbations to the spring harmonic well by water ordering near calcite and Barite surfaces.[35] On the basis of the idea of parsing the force profile into smaller sections,[36] researchers stitched together many measurements, similar to Cleveland's, at different tip−surface distances to reconstruct an interaction profile.[37,38] The best method subtracted the harmonic contribution from the cantilever to produce potential sections, but the constant C is different for each potential section because the measurement process measures relative energy, thus making reconstruction difficult. No clear method for objectively determining the constant has been presented, and miscalculation leads to significant errors in the reconstruction since errors are propagated along the reconstructed profile. The problem is accentuated by instrument noise, which broadens the probability distributions and underestimates the interaction stiffness, which in turn further introduces errors that are propagated along the energy profile. A method for compensating instrument noise and accurately calculating the constant, C, is needed for making reconstruction of the force profile from thermal noise useful, especially for the investigation of high stiffness interactions such as interfacial solvent structure, ligand−receptor binding, and protein folding landscapes.

The high stiffness interaction of solvent structure is of great interest to numerous fields from tribology to protein folding.[39] SFA measurements first observed solvent structure for octamethyl-cyclotetrasiloxane (OMCTS)[40] and continued the investigation of confined liquids for numerous liquids under many conditions.[41−48] More recently, the AFM has been used since

(16) Evans, E.; Leung, A.; Hammer, D.; Simon, S. *Proc. Natl. Acad. Sci. U.S.A.* **2001**, *98*, 3784−3789.
(17) Carrion-Vazquez, M.; Oberhauser, A. F.; Fowler, S. B.; Marszalek, P. E.; Broedel, S. E.; Clarke, J.; Fernandez, J. M. *Proc. Natl. Acad. Sci. U.S.A.* **1999**, *96*, 3694−3699.
(18) Jarzynski, C. *Phys. Rev. Lett.* **1997**, *78*, 2690−2693.
(19) Liphardt, J.; Dumont, S.; Smith, S. B.; Tinoco, I.; Bustamante, C. *Science* **2002**, *296*, 1832−1835.
(20) Hummer, G.; Szabo, A. *Proc. Natl. Acad. Sci. U.S.A.* **2001**, *98*, 3658−3661.
(21) Todd, B. A.; Eppell, S. J.; Zypman, F. R. *Appl. Phys. Lett.* **2001**, *79*, 1888−1890.
(22) Todd, B. A.; Eppell, S. J. *Langmuir* **2004**, *20*, 4892−4897.
(23) Todd, B. A.; Eppell, S. J. *J. Appl. Phys.* **2003**, *94*, 3563−3572.
(24) Derjaguin, B. V.; Rabinovich, Y. I.; Churaev, N. V. *Nature* **1978**, *272*, 313−318.
(25) Joyce, S. A.; Houston, J. E. *Rev. Sci. Instrum.* **1991**, *62*, 710−715.
(26) Thomas, R. C.; Houston, J. E.; Michalske, T. A.; Crooks, R. M. *Science* **1993**, *259*, 1883−1885.
(27) Thomas, R. C.; Tangyunyong, P.; Houston, J. E.; Michalske, T. A.; Crooks, R. M. *J. Phys. Chem.* **1994**, *98*, 4493−4494.
(28) Stewart, A. M.; Parker, J. L. *Rev. Sci. Instrum.* **1992**, *63*, 5626−5633.
(29) Jarvis, S. P.; Yamada, H.; Yamamoto, S.-I.; Tokumoto, H.; Pethica, J. B. *Nature* **1996**, *384*, 247−249.
(30) Jarvis, S. P.; Dürig, U.; Lant, M. A.; Yamada, H.; Tokumoto, H. *Appl. Phys. A* **1998**, *66*, S211−S213.
(31) Thomas, R. C.; Houston, J. E.; Crooks, R. M.; Kim, T.; Michalske, T. A. *J. Am. Chem. Soc.* **1995**, *117*, 3820−3834.
(32) Yamamoto, S.-i.; Yamada, H.; Tokumoto, H. *Rev. Sci. Instrum.* **1997**, *68*, 4132−4136.
(33) Ashby, P. D.; Chen, L. W.; Lieber, C. M. *J. Am. Chem. Soc.* **2000**, *122*, 9467−9472.
(34) Ashby, P. D. Ph.D. Thesis, Harvard University, Cambridge, MA, 2003.
(35) Cleveland, J. P.; Schaffer, T. E.; Hansma, P. K. *Phys. Rev. B* **1995**, *52*, R8692−R8695.
(36) Rabe, U.; Janser, K.; Arnold, W. *Rev. Sci. Instrum.* **1996**, *67*, 3281−3293.
(37) Heinz, W.; Antonik, M. D.; Hoh, J. H. *J. Phys. Chem. B* **2000**, *104*, 622−626.
(38) Willemsen, O. H.; Kuipers, L.; Werf, K. O. v. d.; Grooth, B. G. d.; Greve, J. *Langmuir* **2000**, *16*, 4339−4347.
(39) Sorenson, J. M.; Hura, G.; Soper, A. K.; Pertsemlidis, A.; Head-Gordon, T. *J. Phys. Chem. B* **1999**, *103*, 5413−5426.
(40) Horn, R. G.; Israelachvili, J. N. *J. Chem. Phys.* **1981**, *75*, 1400−1411.
(41) Pashley, R. M.; Israelachvili, J. N. *Nature* **1983**, *306*, 249−250.
(42) Christenson, H. K.; Horn, R. G. *Chem. Scr.* **1985**, *25*, 37−41.
(43) Israelchvili, J. N. *Acc. Chem. Res.* **1987**, *20*, 415−421.
(44) Christenson, H. K. *J. Dispersion Sci. Technol.* **1988**, *9*, 171−206.

the small probe resembles the microscopic asperities that are the points of contact for real materials.[49−53] Long chain alkanes are of particular importance in petroleum lubrication research,[54] and early SFA studies show that long chain alkanes lay down on the mica surface such that the periodicity is ~5 Å (the width of the molecules) and the number of layers is correlated with the chain length of the molecule.[46] Unfortunately, the SFA normalized spring stiffness is very low such that only negative stiffness regions of the force profile are measured and the data are sparse. An AFM experiment using *n*-docecanol revealed layering with a periodicity slightly under 4 Å, but as a result of the noise, the measurement yielded little information about the solvent structure.[50] Discerning details about the equilibrium structure and dynamics of interfacial solvent requires precise measurements that can probe high stiffness interactions.

In this study, we develop Brownian force profile reconstruction (BFPR) for the robust reconstruction of extremely stiff force profiles. Novel methods solve the previous problems associated with instrument noise and energy section overlap, which enables the accurate reconstruction of force profiles stiffer than the cantilever spring constant. BFPR measured the force profile of structured 1-nonanol near hydrophobic surfaces. The profile is continuous until a tip−surface distance of four molecular layers with a maximum stiffness of 5 N/m using a 3.0 N/m cantilever with a radius of curvature of 10 nm.

Experimental Section

Brownian Force Profile Reconstruction. BFPR is a data collection and analysis technique that accurately reconstructs the force profile using the cantilever thermal noise, Brownian motion, to probe the tip−surface interaction. The steps involved in BFPR are as follows. (a) The deflection during a force curve measurement is sampled at least four times the resonant frequency, f_0, which makes the highest frequency component or Nyquist frequency two times f_0, so that the whole resonance and all the thermal motion are included in the measurement. (b) The force curve is parsed into many small sections, on order of 10 000 points each. Each section is binned into a histogram to calculate cantilever deflection probability density. (c) The inverse of Boltzmann's distribution equation, eq 1, converts the cantilever deflection probability density into relative energy. The sections are clipped on both sides to remove the points that have zero probability. A quadratic curve is fit to an energy section without tip−surface interaction to calculate the spring harmonic well. (d) The resulting fit is subtracted from each energy section, and the sections are subsequently scaled for tip−surface distance, derived from the overall deflection of the cantilever and the position of the cantilever support relative to the sample. (e) The energy sections do not overlap because the arbitrary constant C in eq 1 is unknown. Calculating the force by taking the derivative removes the necessity of obtaining C and automatically calculates the proper scaling. (f) All force sections are averaged together using clever weighting methods developed by Willemsen[38] to produce the reconstructed Brownian force profile.

Noise Compensation. Deconvoluting the cantilever deflection distribution from the instrument noise greatly increases the accuracy of BFPR. Gaussian distributions follow the simple relationship that the variance of a sum of distributions is the sum of the variances of the individual distributions,

$$\sigma_m^2 = \sigma_s^2 + \sigma_n^2 \tag{2}$$

where σ_m, σ_s, and σ_n are the standard deviations of the measured signal (sum of distributions), the pure signal, and the noise, respectively. The variance is the square of the standard deviation. If the instrument noise standard deviation is known, σ_n, then the true standard deviation of the cantilever, σ_s, is calculated by assuming that the cantilever thermal noise is Gaussian and using the measured standard deviation, σ_m, in eq 2. The veracity of assuming the distributions are Gaussian is addressed in the Discussion section. Estimations for the instrument noise, σ_n, are obtained by measuring the deflection when the tip is in hard contact with the surface, where the signal is dominated by instrument noise since the contact region stiffness is extremely high, or by calculating a distribution from an independent measurement of the spring constant and the spring constant calculated from the noncontact region of the experiment. Deflection distributions are scaled using a factor,

$$S = \frac{\sqrt{|\sigma_m^2 - \sigma_n^2|}}{\sigma_m} \tag{3}$$

derived from eq 2. Subtracting the average deflection before scaling and subsequently adding the value after the thermal noise is adjusted protects the absolute force information. Probing attractive interactions slightly stiffer than the spring constant leads to bimodal probability density distributions. Compensating the instrument noise requires splitting the two distributions and scaling each separately. Separation of the two modes is achieved by duplicating the deflection data set and low pass filtering near 4 kHz to remove the thermal noise but retain the low-frequency hops from one potential minima to another. Sorting the raw data, point by point, with respect to the low passed set causes one distribution to move to the beginning of the data set, which allows separate scaling. After scaling, the two sets are rejoined for the completion of the BFPR algorithm.

Cantilever Trajectory Simulations. Cantilever trajectory simulations produced the force curve data during the development and testing of BFPR. The trajectories were calculated by direct numerical integration of the cantilever wave equation,

$$m\cdot\ddot{z}(t + \Delta t) = F_n + F_i(z(t)) - k\cdot z(t) - b\cdot\dot{z}(t) \tag{4}$$

where t is time, $z(t)$ is cantilever trajectory with its respective derivatives, and m, k, and b are the cantilever parameters mass, spring constant, and damping. $F_i(z)$ is the tip−surface force profile, and F_n is the thermal force noise produced by a Gaussian white noise generator with a standard deviation equal to $\sqrt{4k_BTbB}$, where T is the temperature and B is the bandwidth, $(2\Delta t)^{-1}$. Igor Pro v 4 (Wavemetrics, Lake Oswego, Or) computed the trajectories and the subsequently reconstructed Brownian force profiles.

The simulation for Figure 1 computed the trajectory of a cantilever with $k = 1$ N/m, $f_0 = 25$ kHz, and $Q = 3$, where $f_0 = \sqrt{k/m}$ and $Q = \sqrt{km}/b$ along a force profile described by

$$F(z) = 100\left(\frac{0.1}{z}\right)^6 - 0.0006\left(\frac{0.1}{z}\right)^3 \tag{5}$$

where x is in angstroms. A 6−3 force profile was used to imitate the long-range attractive chemical forces that are poorly described by a van der Waals model.[34] This force profile had a maximum stiffness of 1.58 N/m in the attractive region near 8 Å of tip−surface separation.

(45) Gee, M. L.; Israelachvili, J. N. *J. Chem. Soc., Faraday Trans.* **1990**, *86*, 4049−4058.
(46) Christenson, H. K.; Gruen, D. W. R.; Horn, R. G.; Israelachvili, J. N. *J. Chem. Phys.* **1987**, *87*, 1834−1841.
(47) Klein, J.; Kumacheva, E. *Science* **1995**, *269*, 816−819.
(48) Klein, J.; Kumacheva, E. *J. Chem. Phys.* **1998**, *108*, 6996−7009.
(49) Han, W.; Lindsay, S. M. *Appl. Phys. Lett.* **1998**, *72*, 1656−1658.
(50) O'Shea, S. J.; Welland, M. E. *Langmuir* **1998**, *14*, 4186−4197.
(51) O'Shea, S. J.; Welland, M. E.; Pethica, J. B. *Chem. Phys. Lett.* **1994**, *223*, 336−340.
(52) Jarvis, S. P.; Uchihashi, T.; Ishida, T.; Tokumoto, H.; Nakayama, Y. *J. Phys. Chem. B* **2000**, *104*, 6091−6094.
(53) Franz, V.; Butt, H. J. *J. Phys. Chem. B* **2002**, *106*, 1703−1708.
(54) Drummond, C.; Alcantar, N.; Israelachvili, J. *Phys. Rev. E* **2002**, *66*.

The temperature of the experiment was 300 K, and the time increment was 500 ns. The trajectory was interpolated such that 10^6 points remained, which were sampled at eight times the resonant frequency. BFPR used 200 sections of 20 000 points each binned into histograms with 0.1 Å resolution.

The simulation for Figure 2 used a cantilever with $k = 3$ N/m, $f_0 = 25$ kHz, and $Q = 3$. The force profile is described by

$$F(z) = 2e^{-(z/3.3)} \sin\left(\frac{2\pi z}{3.9} - 0.9\right) \quad (6)$$

which models the exponentially decaying sinusoidal forces of liquid solvent structure. The period of 3.9 Å matches the period of closest packed alkanes, and the 3.3 Å exponential decay rate is similar to the experimental results for nonanol solvent structure. The 0.9 rad phase shift produced a more realistic tip−surface distance value. This force profile had a maximum stiffness of 5.9 N/m near a tip−surface distance of 4 Å. The trajectory was calculated with a 100 ns time increment and the time course was interpolated to obtain a final sampling rate of eight times f_0. Instrument noise was simulated by adding to the cantilever trajectory a time course of Gaussian white noise whose power measured 160 fm/$\sqrt{\text{Hz}}$. The noisy trajectory was parsed into 200 sections with 10 000 points each, and the force profile was reconstructed with and without noise compensation.

Ordinary force profiles were calculated by filtering the deflection at 2 kHz and converting the deflection data to be a function of tip−surface distance.

Sample Preparation. Metalized AFM tips were fabricated by baking FESP cantilevers (Digital Instruments, 2−5 N/m) in a tube furnace at 700 °C overnight to blunt the tip before depositing 7 nm of chromium and 40 nm of gold in a thermal evaporator (Sharon Vacuum, $P_B \approx 7\times10^{-8}$ Torr). Hydrophobic tip surfaces were prepared by immediately placing metalized tips into 1 mM ethanolic solution of 1-hexadecanethiol (Aldrich) to form a self-assembled monolayer. After at least 4 h of SAM formation, the tips were rinsed with pure ethanol, blown dry with nitrogen, and placed in a similarly cleaned AFM liquid cell tip holder. Hydrophobic sample surfaces were prepared by freshly cleaving highly ordered pyrolytic graphite (HOPG). 1-Nonanol (Fluka >99.5% pure) was used as received.

Data Collection and Analysis. The tip holder, surface, and solution were placed in an AFM (Multimode, Digital Instruments), equipped with an E scanner, and modified to achieve a 36 fm/$\sqrt{\text{Hz}}$ baseline noise and less than 10 pm noise in a 1 mHz to 1 kHz bandwidth leading to 26 pm of noise in the 100 kHz bandwidth used for these experiments.[34] After 1 h of equilibration the sample drift was 2−10 Å/s. Data were collected as the tip drifted into the sample, and when contact was observed the surface was stepped 5 nm away. The cantilever thermal noise was continuously recorded at 100 kS/s with 16 bit resolution using a high-speed digitizer (NI5911, National Instruments) and custom Labview software. After completion of the experiment, the tip was removed and imaged in a TEM. The radius of curvature of the single gold grain at the end was found to be 10 ± 2 nm leading to a 12 ± 2 nm radius of curvature probe once the SAM layer thickness was included. Subsequently, an accurate determination of the spring constant, 3.0 ± 0.2 N/m, was made using the thermal noise spectrum in air.[55]

Force curve analysis was performed using Igor Pro and started with the removal of a linear photodiode drift, which was calculated from the noncontact regions. Next, the tip−surface distance was calculated by determining the equal deflection regions in contact and using the distance the surface was stepped away from the tip. The sensitivity was calculated from contact regions, and the deflection was scaled. An instrument noise distribution was created from the spring constant value obtained in air and the noise distribution in the noncontact region. The data were parsed into individual force curves with ~2×10^6 points each. The force curves were subsequently analyzed using the BFPR algorithm using 200 sections composed of 15 000 points each and a histogram bin size of 0.15 Å. Six reconstructed force profiles were combined to produce the final force profile displayed in Figure 3.

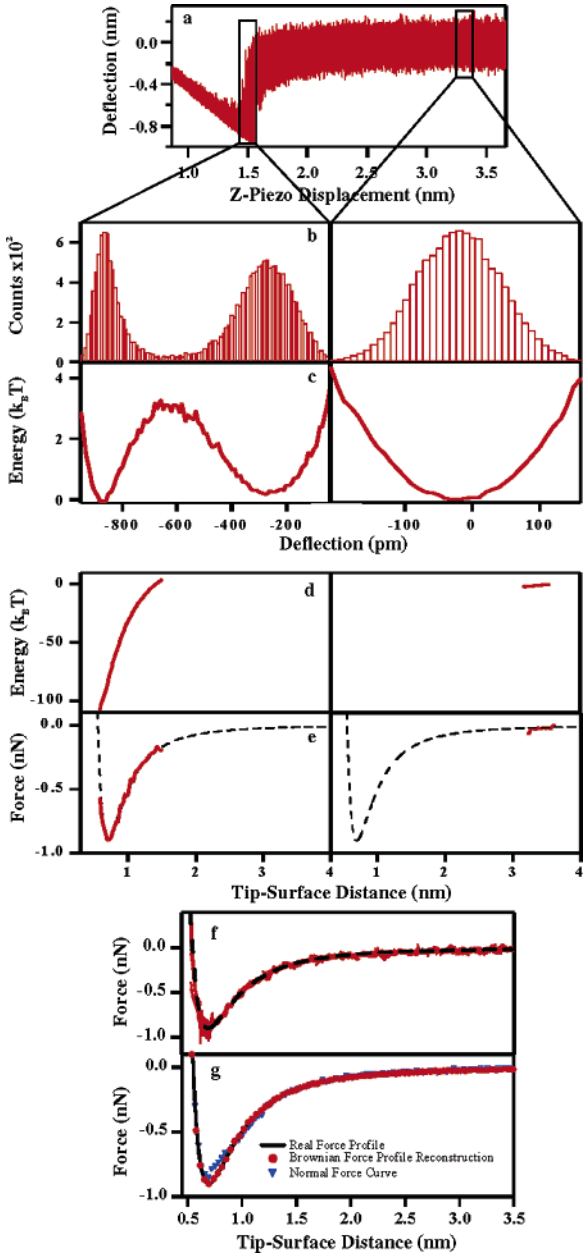

Figure 1. (a) Force curve from simulation trajectory sampled at eight times the resonant frequency to include all cantilever thermal noise. (b) Histograms of sections of force curve marked by boxes in a. (c) Energy sections calculated from histograms using the inverse of the Boltzmann distribution equation. (d) Energy after subtraction of cantilever spring contribution and positioned for tip−surface distance. (e) Force sections (red solid line) calculated from the derivative of energy with the force profile (black dashed line) used in the simulation. (f) All force sections. (g) Averaging the force sections produces the BFPR (red ●), which is more accurate than normal force curve techniques (blue ▼).

Results and Discussion

Simulations. The analysis steps involved in BFPR are illustrated in Figure 1. Figure 1a depicts a simulated trajectory along a simple attractive force profile during a force curve. The utility of BFPR results from harnessing the information content in the thermal noise, and thus sampling at least four times the resonant frequency, f_0, is required such that the first-order

(55) Hutter, J. L.; Bechhoefer, J. *Rev. Sci. Instrum.* **1993**, *64*, 1868−1873.

thermal motion decays before the Nyquist frequency. Oversampling at frequencies greater than eight times f_0 is not productive and adds more instrument noise to the experiment.

The BFPR process follows two different tip−surface interactions in Figure 1b−e to reveal the information content of the thermal noise during analysis. Regions with weak tip−surface interaction are depicted on the right while regions with strong tip−surface interaction are depicted on the left and histograms for these two interactions are shown in part b. The distribution on the right has a single mode and is Gaussian, while the strong tip−surface interaction split the left distribution into two modes. The curvature of each mode is related to the stiffness of the combined potential that region.

Figure 1c contains the relative energy sections calculated from the probability densities using Boltzmann's distribution equation (eq 1). The error in the energy value increased as the number of samples at a specific deflection value in the histogram is decreased, which is very evident in the barrier region on the left side of part c. Large sampling numbers for each section increases precision, because the probabilities calculated from the histograms are more refined, but care must be taken while determining the number of samples in a section so that the tip−surface interaction does not change significantly in the collection window and smear the energy information. Therefore, rather than using enormous sampling numbers for each section, it is more effective to increase the number of sections and have significant overlap between sections to further improve the statistics.

The relative tip−surface potential sections are calculated by subtracting the cantilever harmonic potential and are shown in Figure 1d. Low-frequency deflection within the spring harmonic potential contains most of the force information and is crucial since it determines the tip−surface position and slope of the potential sections. Each potential energy section is a relative measurement, and thus the value of the constant C in eq 1 is unknown, which has been one of the major challenges for thermal reconstruction techniques thus far. Some researchers have tried to maximize the overlap in the tails of the potential sections to obtain C.[37,38] The tails of the distributions are particularly susceptible to errors since the cantilever does not sample these regions often and setting the zero deflection value improperly can introduce a spurious slope to the potential sections. These errors in the potential sections are compounded by the fact that overlapping energy sections propagate the error from one section to another. Thus, using these tails to calculate the value of C invites the introduction of error. We implemented the elegant and robust solution of eliminating the constant through taking the derivative to obtain force information (Figure 1e). As a result, the force section fits perfectly in the force profile without iterative fitting, user input, or the introduction of inaccuracies. Calculation of the force from the potential section increases the noise but averaging of numerous sections restores the precision, and the slight loss in precision is a small cost for the significant increase in accuracy. The last step averages the numerous force sections (Figure 1f) to obtain the reconstructed Brownian force profile (Figure 1g).

BFPR requires precise knowledge of the cantilever position to produce accurate probability distributions. Corruption of the position information by instrument noise severely affects the accuracy of BFPR. Figure 2 displays the results of simulations along an oscillatory force profile (black), which models the forces associated with solvent structure, when 160 fm/$\sqrt{\text{Hz}}$ of instrument noise is added to the deflection. The Brownian force profile without noise compensation, shown in red in part a, replicates the force profile very poorly, compared to normal force profile analysis techniques, shown in blue. Instrument noise degrades the accuracy of the reconstructed force profiles by broadening the probability distributions. The resulting lower estimated stiffness causes the spring constant to be miscalculated, which scales the overall force to a smaller absolute value. More importantly, the inaccurate stiffness for each section causes a systematic tilt to the force sections from lower to higher force as the tip−surface distance is increased. The error can be severe enough to obscure almost all information about the underlying force profile as evidenced by the simulation in Figure 2a.

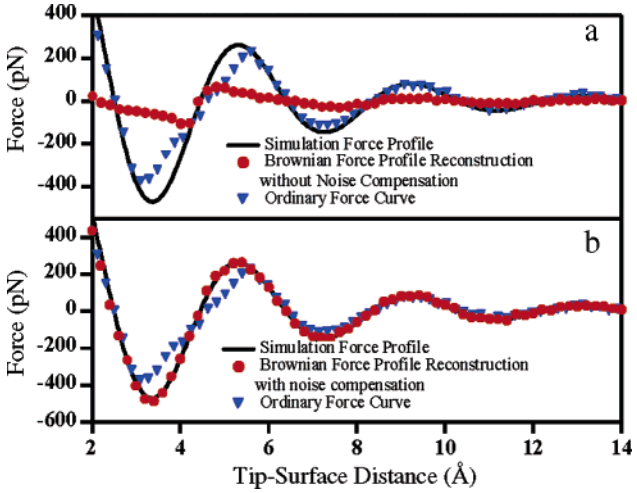

Figure 2. Force profiles reconstructed from simulated trajectories, which include instrument noise, along the true force profile (black solid line). Ordinary force curve techniques (blue ▼) are inaccurate in high stiffness regions. BFPR (red ●) without noise compensation has poor accuracy (a) while noise compensation restores fidelity (b).

We developed a compensation technique that removes the broadening of the deflection distributions caused by instrument noise and restores the fidelity of BFPR through calculating the correct stiffness for each section and cantilever spring constant. BFPR after noise compensation, shown in Figure 2b, more accurately measures the true force profile throughout the whole curve, especially in the positive stiffness regions at 4 and 8 Å. The noise compensation technique solves for the true distribution width from information about the measured and instrument noise distributions since the variance of a sum of signals equals the sum of the variances for Gaussian distributions (eq 2). The assumption that the noise distributions are Gaussian is surprisingly valid since the BFPR algorithm relies upon the tip−surface interaction to distort the thermal noise distribution from Gaussian. The validity originates from the thermal noise more frequently sampling the bottom of the well where the shape is more harmonic. BFPR weighs the frequently sampled regions more highly such that emphasis is placed on the minima in the combined potential energy surface. The local stiffness in these regions modulates the width of the distributions but they stay generally Gaussian. The tails may deviate significantly from a Gaussian shape but they are not weighted heavily. It may seem that the tails of the distributions may be important when they

connect between two distributions for strongly attractive interactions, since the tails are the only measurement of that region. In this situation, the shape of the force profile is mostly determined by the distance between the distributions when the spring harmonic well is removed than the actual population of the tails. Thus, the requirement for Gaussian distributions during noise compensation is relatively loose.

The stark contrast between BFPR with and without noise compensation implies the necessity of an accurate instrument noise measurement, which can be difficult to obtain. Fortunately, BFPR contains an outstanding self-check since the force sections shown in Figures 1f and 4 will not overlap unless the instrument noise distribution, cantilever sensitivity, and z-piezo displacement are correct. Independent measurement of the spring constant, instrument noise, and cantilever sensitivity while confirming overlap of the force sections ensures the accuracy of BFPR.

Experiments probing intermolecular and interfacial force profiles with static deflection of springs can be sorted into three categories depending on the spring stiffness relative to the interaction. The first category is the weak spring limit. As mentioned in the Introduction, most force measurements fall in this category since the measured forces produce large and easily observable displacements. Unfortunately, the stiffer interaction causes a single barrier crossing which passes over the transition region in a few microseconds. Equilibrium information about the tip−surface interaction is difficult to obtain using any analysis method even with averaging of numerous force curves because the total time sampling the transition region is still on the order of tens of microseconds. The opposite category is the stiff spring limit where the spring constant is much greater than interaction stiffness. During measurements, the spring directly probes the equilibrium surface but the deflection is negligible and the information is obscured by instrument noise. Due to the lack of information, researchers have avoided these measurements. Intermediate between these two extremes is the category that probes interactions with spring constants similar to the interaction stiffness.

When the spring constant and the interaction stiffness are similar, then cantilever motion due to thermal excitation becomes very important. Thermal excitations allow the cantilever to hop over shallow barriers and probe regions of the energy landscape other than the local potential of the spring well. Aided by the compensating effect of the spring, the thermal motion causes the probe to move back and forth between regions of strongly attractive interactions and relatively weak interactions. The motion allows the tip to sample the transition region for tens of milliseconds and the proportion of time in each well is exponentially dependent on the relative energy of the wells. Unfortunately, normal force curve techniques place a low pass filter on the deflection signal, which produces the arithmetic mean of the cantilever thermal motion. Since the time in the well is exponentially, not linearly, dependent on energy, the arithmetic mean leads to an overestimation of the attractive forces at tip−surface distances of weak attraction because the average improperly incorporates large deflection values from thermal motion in the strongly attractive region. Similarly, normal force curve techniques lead to underestimation of the force at the bottom of the well because deflections associated with weakly attractive forces are incorrectly incorporated into the average. These errors are apparent in the force profiles produced using normal force curve techniques shown with blue triangles in Figures 1g and 2. These errors render normal force curve techniques inaccurate and less useful in this intermediate range of force measurement. Thus, the only way to probe the true force profile using normal force curve techniques is to work in the stiff spring limit and produce "accurate" results convoluted with noise.

The intermediate category, where normal force curve techniques are inaccurate, is the regime where BFPR becomes most useful. BFPR produces accurate force profiles in this regime because it interprets the motion of the thermal noise and distinguishes between probing highly attractive and weakly attractive regions. BFPR leverages the convolution of the cantilever spring and 3−4 k_BT excursions of the thermal noise to probe potentials up to 100 k_BT deep, as shown in the left side of Figure 1d. In addition, the added energy from the thermal noise allows interactions that are stiffer than the intrinsic cantilever stiffness to be accurately measured. In Figure 1, the interaction is 1.6 N/m while the cantilever is 1 N/m, and in Figure 2, the interaction is 6 N/m while the cantilever is only 3 N/m. Furthermore, the requirement of quasi-equilibrium is loose such that the cantilever may only need to hop over the barrier separating the two wells 5 to 10 times to obtain an accurate reconstruction. Yet, energy barriers between wells increase rapidly as the distance between the wells increases. As the length scale of the interaction increases, the cantilever spring constant must be closer to the true interaction stiffness to achieve quasi-equilibrium. Thus, as researchers seek to probe complex tip−surface interactions that may be composed of numerous force components, they should estimate the total interaction stiffness and length scale and then choose a cantilever stiffness as close as possible to the interaction stiffness with the freedom to have a less stiff spring for short interactions. It is better to err on the side of having too stiff of a cantilever since too weak of cantilever stiffness could require unacceptably long data collection times to reach quasi-equilibrium. The increased accuracy and precision of BFPR will greatly aid the deconvolution of the numerous force components that comprise the tip−surface interaction. Last, since a large gap exists in spring constants that are commercially available between 5 and 20 N/m, the utility of BFPR can be further increased by artificially augmenting the Brownian motion such that it probes more of the energy landscape without increasing sample temperature. The Brownian motion can be increased by driving the cantilever using an external source such as white noise[56] or using Q-control to reduce the effective damping.[34] Externally exciting the cantilever motion effectively increases the cantilever temperature, which will have to be quantified and used in place of ambient temperature in eq 1 during the conversion of probability to energy. Using BFPR in the intermediate category of cantilever stiffness opens up a new paradigm of force measurement since relatively weak springs can be used to obtain accurate results. Thus, BFPR will be a wonderful tool for probing interesting stiff interactions such as protein folding and small molecule ligand interactions.

1-Nonanol. The average of six reconstructed force profiles for 1-nonanol between a graphite surface and methyl-terminated

(56) Koralek, D. O.; Heinz, W. F.; Antonik, M. D.; Baik, A.; Hoh, J. H. *Appl. Phys. Lett.* **2000**, *76*, 2952−2954.

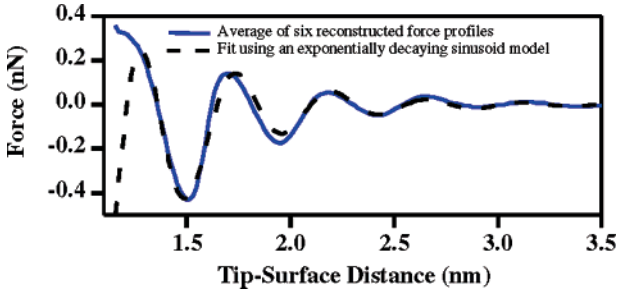

Figure 3. Average of reconstructed force profiles (blue solid line) for 1-nonanol between hydrophobic surfaces and exponentially decaying sinusoidal function (black dashed line). The force profile has a period of 4.5 Å, the molecular diameter of 1-nonanol.

SAM tip is shown in Figure 3 with a fit using an exponentially decaying sinusoid model. The model also includes a monotonic exponential term for the slight long-range attraction. The stiffness in the region between 1.5 and 1.8 nm is 5.4 N/m or 1.8 times greater than the stiffness of the cantilever. BFPR accurately measures the whole force profile for distances greater than 1.4 nm with a fine tip−surface distance increment of 0.15 Å, which has not previously been observed. These accurate and precise results validate the utility of BFPR for measuring stiff force profiles.

The force profile is well fit by a decaying exponential using an oscillation period of 4.5 ± 0.2 Å with the error mainly due to uncertainty in tip−surface distance scale and not the numerical precision of the fit. The excellent fit using the decaying exponential implies the solvent is liquid in this region. Simulations using a nonbonded potential energy minimum of 4.38 Å lead to a spacing of 4.5 Å in the liquid state in perfect agreement with the measured data.[57] The forces were relatively strong, producing normalized forces 10 times stronger than comparable SFA experiments when scaled for the probe radius but similar in magnitude to previous AFM work. In the small probe limit, the Derjaguin approximation, used to normalize the surface forces in SFA experiments, is no longer valid, which could be a source of the discrepancy.[8,58]

Forces experienced by the probe at distances less than 1.4 nm are depicted in Figure 4 using the force sections that comprise force profile reconstructions for two individual force profiles. The region greater than 1.4 nm is sinusoidal but at shorter distances deviations from a sinusoidal force profile suggest the onset of nonliquid behavior. The force profiles contain discontinuities because the interaction stiffness is too high and the cantilever performs a single barrier crossing through to the next layer. The interlayer transition near 1.2 nm is only 3.9 Å. The transition is much smaller than those measured for the fluid layers of 1-nonanol at distances greater than 1.5 nm. We propose that the smaller interlayer distance results from solidification of the 1-nonanol into a hexagonal structure, which would have an interlayer spacing of 3.9 Å for cylinders of radius 4.5 Å. This result is very similar to past SFA experiments, where solidification was also observed for confinement of OMCTS and hexane at six and seven molecular layers, respectively.[47,48] The next transition in Figure 4a is 1.5 Å followed by a 2.6 Å

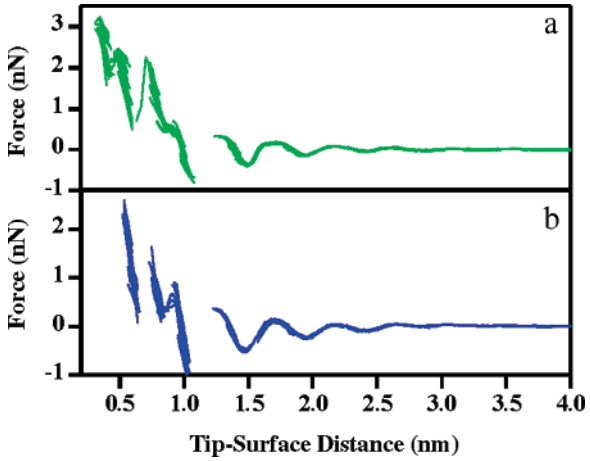

Figure 4. Brownian reconstruction force sections for two force curves a and b of 1-nonanol between hydrophobic surfaces. The force profiles show liquid behavior at distances greater than 1.5 nm and possibly crystalline behavior with crystal orientation rearrangements at distances less than 1.5 nm causing steps only half the molecular width.

step, while Figure 4b has a 1.9 Å step followed by a 2.2 Å step. The sum of the two steps in both curves is 4.1 Å, which is very close to the distance for another molecular layer. A possible interpretation of the smaller step is that the solid changes to a new phase or crystal surface. Rotating the hexagonal lattice by 90° such that the rows of atoms are perpendicular to the surface and the atoms touching the surface are staggered every other layer allows transitions of ∼2 Å.[54] For atomically flat surfaces, the maximum density transition structures lead to a single oscillation for each molecular layer, which is inconsistent with the results presented here. Observation of 2 Å transitions implies that molecular surface roughness is stabilizing rotation of the crystal structure. HOPG is unlikely to have surface roughness, but the headgroup packing of the SAM layer on the tip could stabilize the new crystal orientation since chain packing leads to ordered rows spaced by 5.0 Å with height variations of 1 Å.[59]

Assignment of the exact number of layers between the surfaces is extremely challenging since AFM cannot measure absolute distance, but the last 1.5 Å jump at 0.4 nm in Figure 4a suggests at least 1.5 layers remains. The transition between 1.0 and 1.4 nm should be an integer multiple of layers where the layers are in the energetically most favorable position, parallel with the surface. The transitions between 0.6 and 1.0 nm make another layer. Since the transition from 0.4 to 0.6 in Figure 4a is a half layer, another half layer would be expected before the last full molecular layer. The onset of solid behavior is at a minimum of four molecular layers.

Conclusion

Brownian force profile reconstruction is a robust technique for accurately measuring the whole force profile of strongly attractive intermolecular and interfacial interactions that have previously been inaccessible to other force measurement techniques. Force profiles of liquid 1-nonanol between hydrophobic surfaces reveal liquid ordering for distances greater than four molecular layers and the onset of crystallization followed

(57) Jin, R. Y.; Song, K. Y.; Hase, W. L. *J. Phys. Chem. B* **2000**, *104*, 2692−2701.
(58) Tadmor, R.; Rosensweig, R. E.; Frey, J.; Klein, J. *Langmuir* **2000**, *16*, 9117−9120.
(59) Bain, C. D.; Troughton, E. B.; Tao, Y. T.; Evall, J.; Whitesides, G. M.; Nuzzo, R. G. *J. Am. Chem. Soc.* **1989**, *111*, 321−335.

by possible crystal reorientations upon subsequent confinement. BFPR's ability to measure interactions stiffer than the intrinsic cantilever stiffness will be especially useful for further investigating solvent structure or more biologically relevant interactions such as single ligand−receptor binding and protein folding landscapes.

Acknowledgment. We thank the Air Force Office of Scientific Research for generous support of this work and Liwei Chen, Alex Noy, Tjerk Oosterkamp, Wesley Wong, and Chin Li Cheung for helpful suggestions concerning the manuscript.

JA045970R